Pure crystal field α-mode magnetostriction of the itinerant ferromagnet $Y_2Fe_{14}B$

1999 J. Phys.: Condens. Matter 11 3341

(http://iopscience.iop.org/0953-8984/11/16/015)

J. Phys.: Condens. Matter **11** (1999) 3341–3353. Printed in the UK PII: S0953-8984(99)98091-8

Pure crystal field α-mode magnetostriction of the itinerant ferromagnet $Y_2Fe_{14}B$

C Abadía†, A del Moral†, K Kulakowski†‡ and P A Algarabel†

† Laboratorio de Magnetismo de Sólidos, Departamento de Física de Materia Condensada and Instituto de Ciencia de Materiales de Aragón, Universidad de Zaragoza and Consejo Superior de Investigaciones Científicas, 50009 Zaragoza, Spain

‡ Faculty of Physics and Nuclear Techniques, University of Mining and Metallurgy, al. Mickiewicza 30, 30-059, Krakow, Poland

Received 5 October 1998, in final form 8 February 1999

Abstract. We have experimentally isolated the *pure* single-ion crystal-field origin irreducible magnetostrictive strains $\epsilon^{\alpha,1}$ and $\epsilon^{\alpha,2}$, which respectively represent the volume and the shape c/a ratio distortions, for the tetragonal itinerant ferromagnet $Y_2Fe_{14}B$. The unusual thermal variations of those strains, peaking at about 200 K and decreasing with temperature, have no sensible explanation within the Callen–Callen standard theory of magnetostriction for localized magnetic moments. Instead a developed simple rigid-band Stoner model of magnetostriction for itinerant 3d electrons explains quite well such dependencies and also allows us to extract the *microscopic* magnetoelastic coupling parameters M_{12}^{α} and M_{22}^{α}, accounting for those strains respectively. These parameters are very large, about 10 meV/Fe atom, and of opposite signs.

1. Introduction

The number of itinerant ferromagnets, based on the 3d elements iron, nickel and cobalt, where the *microscopic* magnetoelastic (MEL) coupling parameters of single-ion crystal electric field (CEF) origin, have been determined is really very scarce, in spite of their importance within the subject of ferromagnetism. These parameters take into account the itinerant electron spin–orbit and orbit–lattice interactions, responsible for the MEL coupling. In fact, to our knowledge, only in Ni [1] and in Y_2Fe_{17} [2] have such parameters been neatly determined from experiment. This is by no means a straightforward task because obtaining such MEL parameters from experiment necessitates passing through the development of a theoretical magnetostriction frame model for the 3d-band itinerant electrons. The aims of this work are twofold: to enlarge the meagre number of systems where those MEL parameters are known and, also most interesting, because of the considerable interest of the knowledge of the magnetostriction in the $Y_2Fe_{14}B$ intermetallic. This knowledge is of substantial practical importance because the isomorphous $Nd_2Fe_{14}B$ compound seems, to date, the strongest energy product permanent magnet known for technical applications [3], and, although its magnetostrictive properties were reported some time ago [4], the contribution to the magnetostriction by the Fe sublattice alone was never separated out. Indeed, $Y_2Fe_{14}B$ is the ideal candidate for obtaining such information, as the strongest exchange interaction is within the iron sublattice. It is worthwhile to mention that the magnetostrictive distortions are somewhat larger for $Y_2Fe_{14}B$ than for $Nd_2Fe_{14}B$, and in the case of the c/a ratio tetragonal distortion they are of opposite sign, a result of clearly practical relevance as well.

0953-8984/99/163341+13$19.50

$Y_2Fe_{14}B$ crystallizes in the tetragonal space group $P4_2/mnm$, the Fe atoms occupying six different positions within the unit cell (c, e, j_1, j_2, k_1 and k_2), all of point symmetry lower than $2mm$ [5]. This compound orders ferromagnetically below $T_c = 571$ K [6] and the iron magnetic moment in the six positions ranges from 1.95 to 2.8 μ_B [6, 7]. The hcp structure $\boldsymbol{a}$ [100] and $\boldsymbol{c}$ [001] directions respectively are the magnetically hard and easy axes.

We here report on magnetostriction measurements performed on a single crystal of $Y_2Fe_{14}B$, in applied strong magnetic fields (up to 14 T) and in the temperature range 4.2–400 K, which have allowed us to determine the α-mode irreducible magnetostrictive strains supported by the tetragonal crystalline structure. Those α-strains are two: the volume distortion, i.e. $\epsilon^{\alpha,1} = \epsilon_{xx} + \epsilon_{yy} + \epsilon_z$, and the shape or c/a ratio distortion, $\epsilon^{\alpha,2} = (\sqrt{3}/2)(\epsilon_{zz} - (\epsilon^{\alpha,1}/3))$, where ϵ_{jj} are the Cartesian strains [8]. These strains naturally appear when the average magnetization rotates from the easy axis down to the hard axis and have their origin in the single-ion CEF interaction [8]. However, they are also substantially contributed by the strains developed by the forced magnetization process, which should be present in $Y_2Fe_{14}B$ even during the magnetization rotation process, as we shall see. In this work we present a thorough experimental and theoretical study of the α-mode strictions for $Y_2Fe_{14}B$, where we have been able to separate out such pure single-ion CEF origin magnetostrictions. To our knowledge such an isolation has not been ever reported to the degree of accuracy here attained. A preliminary report about our magnetostriction experiments in $Y_2Fe_{14}B$ was presented elsewhere [9].

A theoretical model was early developed [2] in order to explain and analyse the single-ion CEF magnetostriction in the hexagonal 3d-band itinerant ferromagnet Y_2Fe_{17}. This model has been now successfully applied to the analysis of the magnetostriction of the tetragonal $Y_2Fe_{14}B$ intermetallic, generalizing it somewhat and introducing some quite fruitful modifications. The last outcome of our present work is the extraction of the pure single-ion CEF *microscopic* MEL parameters for $Y_2Fe_{14}B$, which are at the origin of the above mentioned strictions. Not less important is to bring about an explanation of the observed non-monotonic variation of the irreducible strictions with temperature, a classical problem in magnetostriction of 3d metals [10].

The organization of the paper is the following: in section 2 we present the experimental results on the α-mode magnetostriction measurements for $Y_2Fe_{14}B$; in section 3 we deal with the theoretical model of CEF magnetostriction for 3d-band tetragonal systems and the calculations made, and we compare them with the experimental results; in section 4 we extract the results of our work and in section 5 we discuss them and summarize the conclusions.

2. Experimental results: irreducible α-mode magnetostriction for $Y_2Fe_{14}B$

The magnetostriction experiments were performed upon a single crystal of $Y_2Fe_{14}B$. The crystal was grown by the Czochralsky technique, from argon arc-melted buttons of the constituents (at least 99.9% purity). The crystal was cut and x-ray back-Laue oriented with the $(\boldsymbol{c}, \boldsymbol{a})$ and $(\boldsymbol{c}, \boldsymbol{b})$ planes in coincidence with the sample surfaces. The magnetostriction measurements were performed using the well known strain-gauge (SG) technique. The applied strong pulsed magnetic fields (up to 14 T, with pulsed width of $\widetilde{=}$50 ms) were obtained using a capacitor bank, which was discharged into a liquid nitrogen refrigerated copper wound coil. More details of the technique can be found in [11]. In essence we used an AC bridge with two of its arms the SG resistor cemented on the sample and an SG cemented on pure fused silica, in order to correct for unwanted spurious signals, mainly SG magnetoresistance. The overall accuracy of our magnetostriction technique was estimated as $\pm 5 \times 10^{-6}$.

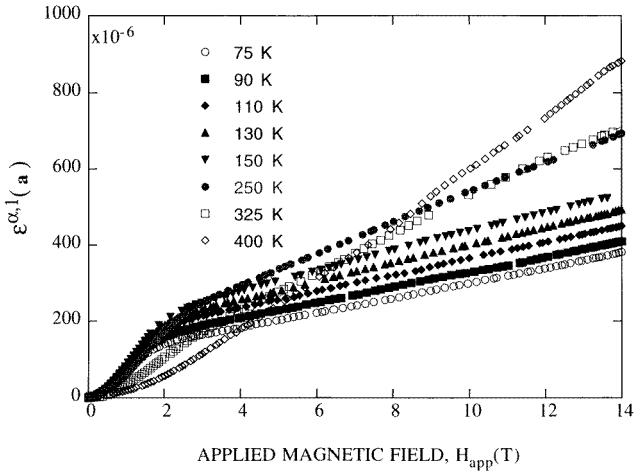

(a)

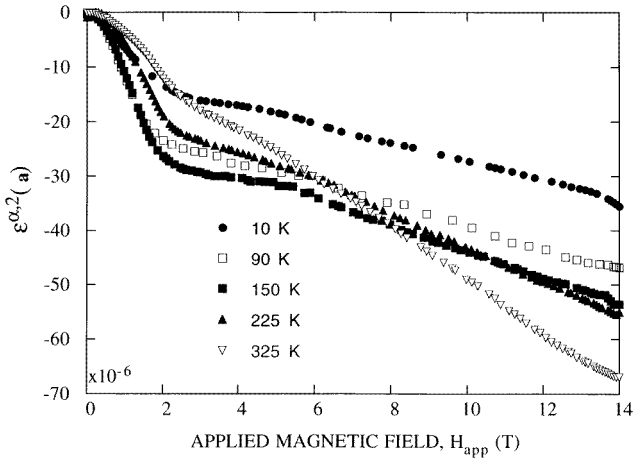

(b)

Figure 1. (a) Isotherms at selected temperatures for the irreducible volume magnetoelastic strain $\epsilon^{\alpha,1}(\boldsymbol{a})$ against applied magnetic field along the hard $\boldsymbol{a}$ axis, for the tetragonal $Y_2Fe_{14}B$ ferromagnet. The 'kinks' correspond to the anisotropy field values, H_K, and beyond them parastriction is developed. (b) As for (a) but for the irreducible strain $\epsilon^{\alpha,2}(\boldsymbol{a})$, which measures the tetragonal distortion (c/a ratio distortion) for the $Y_2Fe_{14}B$ intermetallic.

In order to determine the above mentioned α-strictions, we need to perform two different experiments: applying the magnetic field along the easy $\boldsymbol{c}$ axis and along the hard $\boldsymbol{a}$ axis of the $Y_2Fe_{14}B$ crystal, and each time measuring the strains along the basal plane $(\boldsymbol{a}, \boldsymbol{b})$ axes and along $\boldsymbol{c}$. The expressions relating the irreducible strains to the experimentally measured $\lambda(\phi, \beta)$ strictions (ϕ and β respectively are the applied magnetic field and strain measurements directions) are $\epsilon^{\alpha,1}(\boldsymbol{a}) = \lambda(\boldsymbol{a}, \boldsymbol{a}) + \lambda(\boldsymbol{a}, \boldsymbol{b}) + \lambda(\boldsymbol{a}, \boldsymbol{c})$ and $\epsilon^{\alpha,2}(\boldsymbol{a}) = (1/\sqrt{3})(\lambda(\boldsymbol{a}, \boldsymbol{c}) - (1/2)(\lambda(\boldsymbol{a}, \boldsymbol{a}) + \lambda(\boldsymbol{a}, \boldsymbol{b})))$ [12].

In figures 1(a) and (b) we present the isotherms for $\epsilon^{\alpha,1}(\boldsymbol{a})$ and $\epsilon^{\alpha,2}(\boldsymbol{a})$ ($\boldsymbol{a}$ means the direction of the applied magnetic field). At low temperatures the isotherms show distinctive

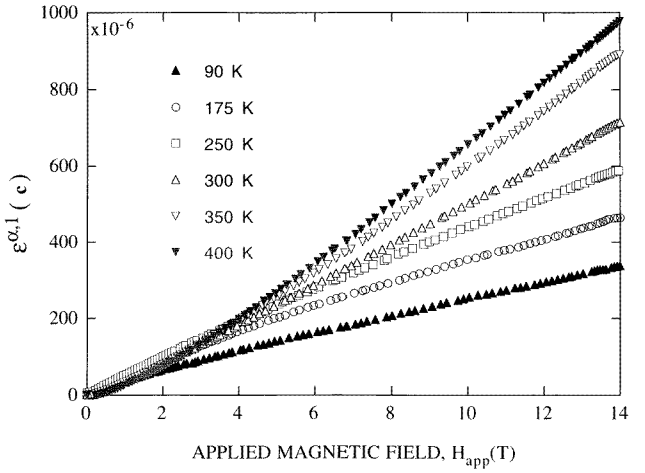

(a)

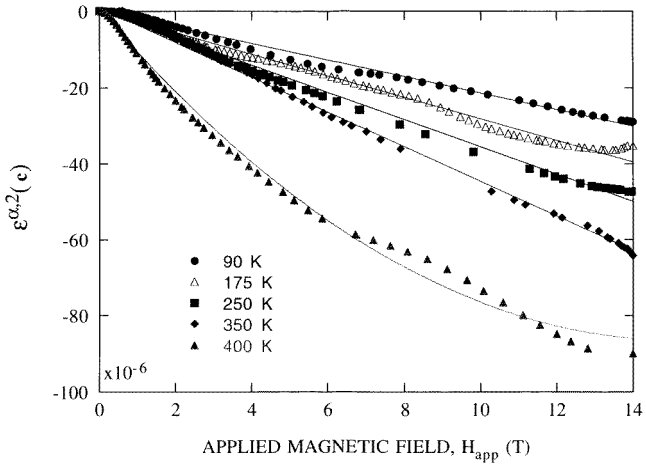

(b)

Figure 2. (a) Isotherms at selected temperatures for the irreducible volume magnetoelastic strain $\epsilon^{\alpha,1}(\boldsymbol{a})$ against applied magnetic field along the easy $\boldsymbol{c}$ axis for the tetragonal $Y_2Fe_{14}B$ ferromagnet. The low temperature almost linear-variation, starting at zero magnetic field, is associated with the magnetization paraprocess. (b) As for (a) but for the irreducible strain $\epsilon^{\alpha,2}(\boldsymbol{a})$, which measures the tetragonal distortion (c/a ratio distortion) for the $Y_2Fe_{14}B$ intermetallic. The lines are eye guides.

'kinks', evolving afterwards almost linearly with field. The fields at the kinks coincide quite well with the measured anisotropy field values $\boldsymbol{H}_K$ [13], where the average magnetization has fully rotated from the $\boldsymbol{c}$ axis down to the $\boldsymbol{a}$ axis against the anisotropy torque. This linear variation is also observed in the $\epsilon^{\alpha,1}(\boldsymbol{c})$ and $\epsilon^{\alpha,2}(\boldsymbol{c})$ isotherms (figures 2(a) and (b)) starting from zero applied field, and because the $\boldsymbol{c}$ axis is easy, $\epsilon^{\alpha,1}(\boldsymbol{c})$ and $\epsilon^{\alpha,2}(\boldsymbol{c})$ can be associated with the forced magnetization or paraprocess mechanism. In this paper we are not interested in the rather difficult theoretical analysis of parastriction, where many-body 3d-electron effects seem to lead to the paraprocess phenomenon [14], and where the extremely difficult analysis of the MEL coupling has not yet been performed.

However a by no means negligible forced magnetostriction contribution, which 'contaminates' the CEF one, is already present in the $\epsilon^{\alpha,1}(\boldsymbol{a})$ and $\epsilon^{\alpha,2}(\boldsymbol{a})$ strains *below* $\boldsymbol{H}_K$ (figures 1(a) and 1(b)). This happens because the strain slopes above $\boldsymbol{H}_K$ are the same for the $\boldsymbol{a}$ and $\boldsymbol{c}$ directions (compare figures 1(a) and 2(a) and figures 1(b) and 2(b), respectively), and because along $\boldsymbol{c}$ the low temperature slopes do not change significantly on crossing the field $\boldsymbol{H}_K$. The existence of parastriction along the rotational magnetization process has not yet been reported, to our knowledge, and it constitutes a intriguing result.

Now, at the field $\boldsymbol{H}_K$ the rotational magnetization process is finished and in order to obtain the *pure* single-ion CEF magnetostrictions we have to subtract from the $\epsilon^{\alpha,1}(\boldsymbol{a})$ and $\epsilon^{\alpha,2}(\boldsymbol{a})$ values at $\boldsymbol{H}_K$ the corresponding parastriction contributions. This can be accomplished by assuming that these contributions are accounted for by $\epsilon^{\alpha,1}(\boldsymbol{c})$ and $\epsilon^{\alpha,2}(\boldsymbol{c})$, as discussed before. Therefore in figures 3 and 4 we respectively show the thermal variations of the pure single-ion CEF strains $\Delta\epsilon^{\alpha,1} \equiv \epsilon^{\alpha,1}(\boldsymbol{a}) - \epsilon^{\alpha,1}(\boldsymbol{c})$ and $\Delta\epsilon^{\alpha,2} \equiv \epsilon^{\alpha,2}(\boldsymbol{a}) - \epsilon^{\alpha,2}(\boldsymbol{c})$, taken at the anisotropy field $\boldsymbol{H}_K$, which is slightly temperature dependent. The variations are rather similar, peaking at about 200 K and decreasing with temperature (figures 3 and 4), being almost proportional to each other. The interesting feature is that these thermal variations are *not* reminiscent at all of the predicted ones by the Callen–Callen standard theory of single-ion CEF magnetostriction for localized electrons, which merely predicts a monotonic decrease of the strictions with increasing temperature [8]. As we shall explain below this more complex variation has its origin in the itinerant character of the iron 3d magnetic moments.

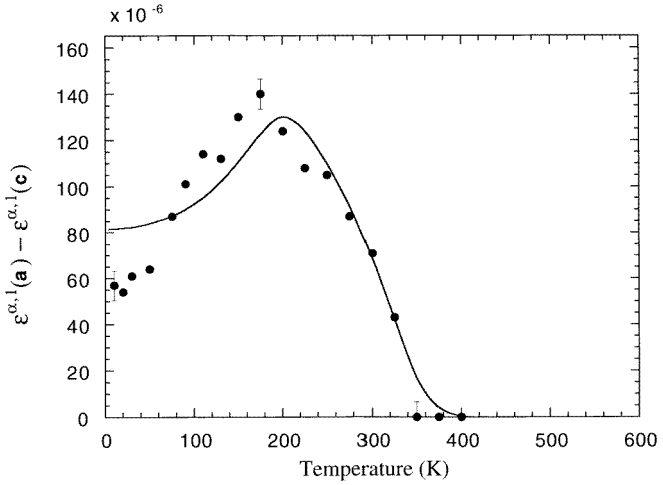

Figure 3. Temperature dependence of the differential irreducible volume strain $\epsilon^{\alpha,1}(\boldsymbol{a}) - \epsilon^{\alpha,1}(\boldsymbol{c})$ for the $Y_2Fe_{14}B$ ferromagnet. Within the parenthesis are shown the applied magnetic field directions. The strain values are for the field values where the isotherms show a 'kink', i.e. at the anisotropy fields $H_K \cong 2$ T (see figure 1(a)). The line is the theoretical model fit, calculated as explained in the text and with the parameters quoted in table 1.

Table 1. Values of the model parameters used for the single-ion CEF magnetostriction calculations in the $Y_2Fe_{14}B$ intermetallic. The meanings of the parameters are explained in the main text. The values for B_{20}, B_{44}, A, M^{α}_{12} and M^{α}_{22} are expressed in eV/Fe atom, and those of Ω_0, Ω_1 and $\delta(0)$ in eV. R and n are dimensionless.

R	B_{20}	B_{44}	Ω_0	Ω_1	n	$\delta(0)$	α	10^3A	$10^3M^{\alpha}_{12}$	$10^3M^{\alpha}_{22}$
0.95	−0.77	±0.41	0.5	0.12	6.7	1.92	0.4	23.4	−18	8.6

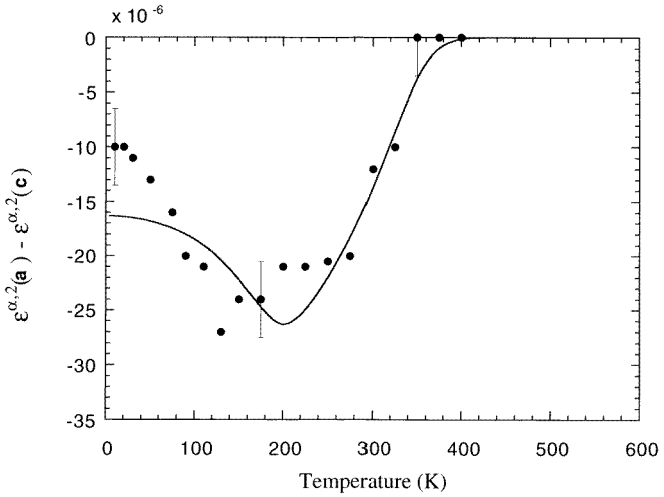

Figure 4. As for figure 3 but for the differential irreducible tetragonal strain $\epsilon^{\alpha,2}(\boldsymbol{a}) - \epsilon^{\alpha,2}(\boldsymbol{c})$. Now the strain values correspond to the 'kinks' of the isotherms of $\epsilon^{\alpha,2}(\boldsymbol{a})$ (see figure 1(b)), i.e. at the anisotropy fields $\boldsymbol{H}_{\mathrm{K}}$ as well. The line is the theoretical model fit, calculated as explained in the text and with the parameters quoted in table 1.

3. Magnetostriction model for itinerant tetragonal ferromagnets

3.1. Model Hamiltonian and energy band splitting

The existence of CEF origin magnetic anisotropy, between the tetragonal $\boldsymbol{c}$ axis and the basal plane [13], and of magnetostriction in $Y_2Fe_{14}B$, must be connected with the existence of orbital degenerate energy levels for the iron 3d-band electrons. However on the grounds of the so low point symmetries for the six Fe sites, the CEF anisotropy vanishes, as the resulting unperturbed Fe energy levels are singlets [8, 15]. Therefore we should have in $Y_2Fe_{14}B$ at least one effective doublet, which can produce both single-ion CEF anisotropy and magnetostriction. This situation may be modelled considering that the six Fe sites are reduced to only one effective site within an average tetragonal symmetry. Therefore in our model we describe the 3d itinerant electrons by Bloch wavefunctions within the tight-binding approximation, and moving around within such a symmetry. For tetragonal symmetry the splitting by the CEF becomes [8, 15]: an orbital doublet, with wavefunctions $\{|xz\rangle, |yz\rangle\}$, and three orbital singlets, with wavefunctions $|xy\rangle$, $|x^2 - y^2\rangle$ and $|2z^2 - x^2 - y^2\rangle$. Our starting wavefunction basis is constituted by these orbital states, adding to them the spin states $|\pm 1/2\rangle$, i.e. ten states overall. Summarizing our model works within the tight-binding approximation, using Bloch functions of the usual kind, $|\boldsymbol{k}; \nu\rangle$ [16], where $\boldsymbol{k}$ is the electron wave-vector and ν, the orbital plus spin state.

The overall itinerant 3d-electron Hamiltonian at the electron lattice point $\boldsymbol{r}$ can be modelled in the followin way:

$$H(\boldsymbol{r}) = H_{\mathrm{CF}} + H_z + H_{\mathrm{so}} + H_{\mathrm{me}} + H_{\mathrm{el}} \tag{1}$$

where the different Hamiltonians are explained below. They all refer to a single ion, as the matrix elements $\langle \boldsymbol{k}'; \nu' | H | \boldsymbol{k}; \nu \rangle$ can be readily shown to be $\boldsymbol{k}$ independent. Now, for tetragonal symmetry the *simplest* CEF Hamiltonian giving one orbital doublet and three orbital singlets, within the above basis, is

$$H_{\mathrm{CF}} = B_{20} O_{20} + B_{44} O_{44} \tag{2}$$

where the term in B_{44} is the smallest order one to have a tetragonal CEF. The energy levels ensuing from Hamiltonian (2) are: $-\Delta_{20}$ for the doublet, and $\{-2\Delta_{20},\ 2\Delta_{20} - \Delta_{44}$ and $2\Delta_{20} + \Delta_{44}\}$ for the singlets, where $\Delta_{20} \equiv 3B_{20}$ and $\Delta_{44} \equiv 12B_{44}$. O_{20} and O_{44} are Stevens operators of the orbital angular momentum, $\boldsymbol{L}$ [17]. The CEF parameters B_{20} and B_{44} for $Y_2Fe_{14}B$ have not been reported, and therefore should be adjusted within our magnetostriction calculations. Adding in equation (2) the next tetragonal term $B_{40}O_{40}$ [15] increases the number of CEF parameters to be adjusted without modifying qualitatively the kind of splitting. In fact we will see that this approximation works quite well when comparing our model results with the magnetostriction experiments in $Y_2Fe_{14}B$.

The Zeeman term is composed of spin and of orbital contributions, which within the mean field approximation and under an effective magnetic field, $\boldsymbol{H}_{\rm eff}$, of exchange origin (for the numerical calculations the external field, $\boldsymbol{H}_{\rm app.}$, is assumed to be zero, as we are calculating almost spontaneous strictions for $H_{\rm K} \ll H_{\rm eff}$), can be written as

$$H_z = \mu_B(\boldsymbol{\sigma} + \alpha \boldsymbol{L}) \cdot \boldsymbol{H}_{\rm eff} \tag{3}$$

where σ are the Pauli matrices, α, a parameter to introduce the effective CEF quenching of the momentum $\boldsymbol{L}$ and also the effect of the orbital polarization [18] by $\boldsymbol{H}_{\rm eff}$. The spin–orbit (SO) contribution has the usual form

$$H_{\rm so} = A\boldsymbol{L} \cdot \boldsymbol{\sigma} \tag{4}$$

where A is the SO coupling constant.

The CEF single-ion magnetoelastic coupling Hamiltonian, up to second-order terms, has the form [2, 8]

$$H_{\rm me} = -\sum_{i=1,2}\left[M^{\alpha}_{i1}[L_x^2 + L_y^2 + L_z^2] + \frac{\sqrt{3}}{2}M^{\alpha}_{i2}[L_z^2 - \tfrac{1}{3}L(L+1)]\right]\epsilon^{\alpha,i} \tag{5}$$

where M^{α}_{ij} $(i, j = 1, 2)$ are the *microscopic* MEL coupling parameters and $\epsilon^{\alpha,i}$ the irreducible strains. The classical elastic energy, $H_{\rm el}$, in terms of the symmetry elastic constants C^{α}_{ij} can be found elsewhere [8].

A full analytical diagonalization of the Hamiltonian H was performed. Because the CEF energy is much greater than the SO one, we introduced the simplifying assumption of neglecting the matrix elements of the SO interaction between the doublet and the singlets and among the singlets themselves. As in the experiment, we align the effective magnetic field, $\boldsymbol{H}_{\rm eff}$, parallel and perpendicular ($\boldsymbol{a}$ axis) to the $\boldsymbol{c}$ axis. The energy levels, E_λ, and corresponding wavefunctions, $|\lambda\rangle$, are readily obtained and we omit giving here their specific expressions for the sake of conciseness. The level expressions are similar in structure to the ones that we obtained before for the Y_2Fe_{17} compound [2], differing only because of the different CEF symmetries, i.e. hexagonal in Y_2Fe_{17}. They are functions of: the CEF parameters B_{20} and B_{44}, A, α, $\boldsymbol{H}_{\rm eff}$ (or equivalently of the Stoner gap, $\delta = (M_+ - M_-)H_{\rm eff}$, where $\pm$ refer to the spin polarizations) and, most important, the MEL energy. The MEL contributions to the *diagonalized* Hamiltonian H (equation (1)) energy levels are linear functions of the MEL parameters M^{α}_{ij} and the strains $\epsilon^{\alpha,i}$, and are given in appendix A. Within our model, the ten 3d energy levels, E_λ (λ = 1–10), are respectively the centres of ten narrow elliptical shaped bands [19] with densities of states $\rho_\lambda(E)$ and half-bandwidths Ω_λ. To these orbital bands we add two 'wide' (of Ω_0 half-bandwidth) non-orbital bands with spins up and down, coming from itinerant electrons of other characters than 3d, and whose centres are therefore determined by the spin only Zeeman coupling (these bands are numbered by $\lambda = 11, 12$ respectively).

3.2. Magnetostriction α-mode calculations

The calculation of the strictions $\epsilon^{\alpha,1}$ and $\epsilon^{\alpha,2}$ in the $Y_2Fe_{14}B$ intermetallic passes by evaluating the distortion of the 3d-band electronic structure produced by the strains. In order to perform such a formidable task some reasonable simplifications should be introduced within our model calculations. First it is well known that the main contribution to MEL coupling comes from a few high symmetry $\boldsymbol{k}$-points in the tetragonal Brillouin zone [20]. This is so because those $\boldsymbol{k}$-states are degenerate or nearly so [21]. Now, such a degeneracy is lifted out by the strong Zeeman and the weaker SO interactions and henceforth mixed states of non-null average orbital angular momentum $\langle \boldsymbol{L} \rangle$ will appear. Therefore those states can give rise to magnetostriction. The second condition is that such $\boldsymbol{k}$-points must be close enough to the Fermi surface, as in the other case $\boldsymbol{L}$ is fully quenched, because of the orbital interband electron hopping between Fe sites [21]. Specifically, it will be enough to consider only one $\boldsymbol{k}$-point along the $\boldsymbol{c}^*$-axis of the tetragonal Brillouin zone, and close to the Fermi wavevector, $\boldsymbol{k}_F$, in order to get the $|\boldsymbol{k}; \lambda\rangle$ states ($\lambda = 1$–4, coming from the $\{|xz\rangle, |yz\rangle\}$ doublet) partially unoccupied (fully occupied levels are indeed magnetostrictively inert, as the average $\langle \boldsymbol{L} \rangle = \boldsymbol{0}$).

It was early shown [2] that under applied magnetic field and resulting induced strains, and within the Stoner rigid band approximation, the variation of the relevant magnetic free energy (i.e. resulting from non-null $\langle \boldsymbol{L} \rangle$ levels), $U_m(\boldsymbol{H}_{eff}, \epsilon^{\alpha,i})$ is given by the model expression

$$\Delta U_m = -\sum_{\lambda=1}^{10} n_\lambda \Delta E_\lambda \tag{6}$$

where ΔE_λ are the band-centre energy shifts produced by those agents, and

$$n_\lambda = \int_{-\infty}^{\mu} \rho_\lambda(E)\, \mathrm{d}E \tag{7}$$

is the λth-band electron number, with the constraint $\sum_{\lambda=1}^{12} n_\lambda = n$, n being the total number of electrons per Fe atom (3d ones and itinerant electrons of other characters [22]; only the 3d bands, with $\lambda = 1$–10, will indeed contribute to U_m in equation (6)). μ is the chemical potential, which was determined from the above constraint equation (7), as we shall see below.

From equation (6) one immediately obtains the relations

$$\frac{\partial U_m}{\partial \epsilon^{\alpha,i}} = -\sum_{\lambda=1}^{10} n_\lambda \frac{\partial E_\lambda}{\partial \epsilon^{\alpha,i}} \qquad (i = 1, 2). \tag{8}$$

Then from equation (8) and equations (A1)–(A3) of appendix A we specifically obtain

$$\frac{\partial U_m}{\partial \epsilon^{\alpha,i}} = 6M^\alpha_{i1} S_\lambda - \sqrt{3} M^\alpha_{i2} W_\lambda \qquad (i = 1, 2) \tag{9}$$

where

$$S_\lambda = \sum_{\lambda=1}^{10} n_\lambda \tag{10a}$$

$$W_\lambda = \frac{1}{2}\sum_{\lambda=1}^{4} n_\lambda - \sum_{\lambda=5}^{8} n_\lambda + \sum_{\lambda=9}^{10} n_\lambda. \tag{10b}$$

Notice that S_λ and W_λ depend on the $\boldsymbol{H}_{eff}$ orientation within the unit cell, because n_λ depends on $\boldsymbol{H}_{eff}$, according to equation (7). Also, S_λ is embodied in the magnetostriction calculation because it is not quite the 3d electron number n, but it results from the number of electronic states with unquenched $\boldsymbol{L}$. We will come back afterwards to this point.

Now, in order to obtain the equilibrium strains, $\bar{\epsilon}^{\alpha,i}$, in terms of the *microscopic* MEL parameters, one needs to add to $U_{\rm m}$ the classical elastic energy $U_{\rm el}$ and minimize $U_{\rm m} + U_{\rm el}$ against the strains. One obtains

$$\bar{\epsilon}^{\alpha,i} = \frac{1}{\Delta_\alpha}\left[C^\alpha_{jj}\left(-\frac{\partial U_{\rm m}}{\partial \epsilon^{\alpha,i}}\right) - C^\alpha_{12}\left(-\frac{\partial U_{\rm m}}{\partial \epsilon^{\alpha,j}}\right)\right] \qquad i,\, j = 1, 2;\; j \neq i \tag{11}$$

with $\Delta^\alpha \equiv C^\alpha_{11}C^\alpha_{22} - (C^\alpha_{12})^2$. One has to distinguish between $U_{\rm m}$, for $\boldsymbol{H}_{\rm eff}$ parallel ($\|$) and perpendicular $\perp$ to the $\boldsymbol{c}$ axis. From equations (9) and (11) we immediately obtain the expressions for the equilibrium strains,

$$\bar{\epsilon}^{\alpha,1}(p) = A^\alpha_{11}S_\lambda(p) + A^\alpha_{12}W_\lambda(p) \tag{12a}$$

$$\bar{\epsilon}^{\alpha,2}(p) = A^\alpha_{21}S_\lambda(p) + A^\alpha_{22}W_\lambda(p) \tag{12b}$$

where p stands for the considered two $\boldsymbol{H}_{\rm eff}$ orientations, parallel ($p = \|$) and perpendicular ($p = \perp$) to the $\boldsymbol{c}$ axis. The $A_{ij}(p)$ parameters, in equations (12), which embody the wanted microscopic MEL parameters, are given in appendix B. The thermal dependencies of the strains are embodied within the functions $S_\lambda(p)$ and $W_\lambda(p)$, which in turn depend on the temperature dependent Stoner gap, δ, through the spontaneous magnetization, $M_s(T)$ (see section 3.1 for the δ expression).

4. Results

Apparently we have at our disposal four irreducible strains, i.e. $\epsilon^{\alpha,i}(\boldsymbol{a})$ and $\epsilon^{\alpha,i}(\boldsymbol{c})$, with $i = 1, 2$, in order to eventually determine the four MEL parameters M^α_{ij}. But the $\epsilon^{\alpha,i}(\boldsymbol{a})$ strains are contaminated with forced magnetostriction even for fields $H < H_{\rm K}$. However, as our model is only suitable for the theoretical analysis of the pure single-ion CEF magnetostriction, we have to compare the model equations (12) with the two differential strains $\Delta\epsilon^{\alpha,1}$ and $\Delta\epsilon^{\alpha,2}$, i.e. removing the forced striction, as discussed in section 2. But this procedure does not remedy our problem of determining four MEL parameters from the two $\Delta\epsilon^{\alpha,1}$ and $\Delta\epsilon^{\alpha,2}$ strains. However, from figures 3 and 4 we can observe that $\Delta\epsilon^{\alpha,1}$ and $\Delta\epsilon^{\alpha,2}$ are proportional to each other, within the experimental error, in the range of temperatures studied. Looking at equations (12) this proportionality is a strong indication that $S_\lambda(\|) \cong S_\lambda(\perp) = S_\lambda$, insofar as these non-null $\langle \boldsymbol{L} \rangle$ electron band fillings do not differ too much for the two $\boldsymbol{H}_{\rm eff}$ orientations, as our detailed calculations reveal. Still we have four unknowns in equations (12). We cannot set out $M^\alpha_{11} = M^\alpha_{21} = 0$, as according to equation (5) they have CEF contributions. However a further reasonable approximation that can be made is to assume that the two irreducible α-modes are decoupled, i.e. we set out $C^\alpha_{1,2} \cong 0$. Introducing all those simplifications in equations (12) we finally obtain

$$\Delta\epsilon^{\alpha,1} \equiv \epsilon^{\alpha,1}(\boldsymbol{a}) - \epsilon^{\alpha,1}(\boldsymbol{c}) = \frac{\sqrt{3}M^\alpha_{12}}{C^\alpha_{11}}[W_\lambda(\perp) - W_\lambda(\|)] \tag{13a}$$

$$\Delta\epsilon^{\alpha,2} \equiv \epsilon^{\alpha,2}(\boldsymbol{a}) - \epsilon^{\alpha,2}(\boldsymbol{c}) = \frac{\sqrt{3}M^\alpha_{22}}{C^\alpha_{22}}[W_\lambda(\perp) - W_\lambda(\|)]. \tag{13b}$$

In figures 3 and 4 we present the fits by the theoretical model equations (13) to the experimentally obtained thermal variations of the differential strains $\Delta\epsilon^{\alpha,1}$ and $\Delta\epsilon^{\alpha,2}$. Overall the agreement obtained can be reported as rather satisfactory. Our target is to obtain the MEL parameters M^α_{12} and M^α_{22}. However nothing is known about the elastic stiffness constants C^α_{ii} for $Y_2Fe_{14}B$; we only dispose of the elastic bulk, B, and shear, G, moduli as determined for polycrystalline samples [23]. It can be shown that the symmetry elastic constants are related to them in the way $C^\alpha_{11} \cong B \cong 12.5$ eV/Fe atom and $C^\alpha_{22} \cong 4G \cong 30$ eV/Fe atom, values at 0 K;

they vary slightly with temperature up to $T_c \cong 571$ K [23]. The values of the model parameters used in the fits are collected in table 1. The quoted values of R, B_{20}, B_{44}, Ω_0, Ω_1, M_{12}^{α} and M_{22}^{α} are the result of the fits of the thermal variations of $\Delta\epsilon^{\alpha,1}$ and $\Delta\epsilon^{\alpha,2}$, although we started the fits with some parameters (R, B_{20}, B_{44}, Ω_0 and Ω_1 and α), previously found for the also axial itinerant iron-rich ferromagnet Y_2Fe_{17} [2]. The ratio between the filling capacities [19] of the elliptical wide conduction band and the five 3d-electron narrower bands is given by R. The value of A is the SO coupling parameter for metallic iron [1]. We fixed the total number of electrons within the 3d bands and other characters itinerant bands to be $n = 6.7$ per Fe atom, as resulting from polarized band structure calculations [22]. The 0 K Stoner gap was also taken from the same calculations [22]. As mentioned in sections 3.1 and 3.2, δ was allowed to change with temperature according to the temperature variation of the spontaneous magnetization M_s [24]. Then the resulting Fermi level as obtained from the constraint equation (7) amounts to $\mu(0) = 1.73$ eV at 0 K, measured from the unsplit wide-band bottom. It became slightly temperature dependent in order to keep the total number of electrons fixed, $n = 6.7$ [22] (the variation of $\mu = \mu(T)$ was about -10% in the temperature range from 4.2 to 400 K).

The second major issue of this work is related to the obtention of the CEF and MEL parameter values. For $Y_2Fe_{14}B$, B_{20} is of the same order of magnitude as for Y_2Fe_{17} and of opposite sign ($B_{20} = 1.23$ eV/Fe atom for Y_2Fe_{17}) [2], i.e. in good agreement with $\boldsymbol{a}$ being in the latter compound the easy axis (planar) and the $\boldsymbol{c}$ axis in $Y_2Fe_{14}B$ (axial). It is worth noticing that the B_{20} value is about three orders of magnitude smaller ($B_{20} \approx -0.2$ meV/ion) [12] for the Nd^{3+} ion in the *isomorphous* compound $Nd_2Fe_{14}B$ and of the same sign. The much larger value of B_{20} for the Fe atom is a consequence of the expected very intense CEF gradient, A_{20} ($B_{20} = \alpha_L A_{20}\langle r^2\rangle_{3d}$, where α_L is the Stevens reduced matrix element and $\langle r^2\rangle_{3d}$, the 3d shell radial quadratic moment), felt by the Fe atom in transition metal intermetallic compounds at sites of low point symmetry, because of the much weaker 3d-electron shell CEF shielding. However magnetocrystalline anisotropy energy is weaker (anisotropy field $H_K \cong 1.8$ T at 4.2 K) in $Y_2Fe_{14}B$ than in $Nd_2Fe_{14}B$ ($H_K \cong 17$ T at 4.2 K) [7] because of the strong quenching of the angular orbital momentum $\boldsymbol{L}$ in the former. It is noticeable that we found the sign of $B_{44} = \pm 0.41$ eV/Fe atom to be irrelevant as it produces the same calculated $\Delta\epsilon^{\alpha,1}$ and $\Delta\epsilon^{\alpha,2}$ values, in good agreement with the negligible basal plane magnetocrystalline anisotropy found in $Y_2Fe_{14}B$ [7].

The signs of M_{12}^{α} and M_{22}^{α} are *opposite* because the $\Delta\epsilon^{\alpha,1}$ and the $\Delta\epsilon^{\alpha,2}$ differential strains have opposite signs. This is also a peculiar feature of magnetoelastic coupling in many anisotropic uniaxial rare earth ferromagnets [12]. Also the MEL parameters become larger (between about one and two orders of magnitude) than in strongly anisotropic rare earth intermetallics [12]. Generally this is again a consequence of the stronger CEF felt by the Fe atoms in 3d intermetallics.

5. Discussion and conclusions

We have been able to isolate the *pure* single-ion crystal-field origin magnetostrictive α-strains of volume, $\epsilon^{\alpha,1}$, and tetragonal, $\epsilon^{\alpha,2}$, characters, for the tetragonal itinerant iron rich $Y_2Fe_{14}B$ ferromagnet, data of considerable technological importance. In spite of the simplifications introduced: the assumption of an average tetragonal symmetry for the six low symmetry Fe sites, the assumed simple elliptical band density of states, the accounting for only one $\boldsymbol{k}$-wavevector within the Brillouin zone, the neglect of some matrix elements of the spin–orbit Hamiltonian and the decoupling between the α-modes, our model explains quite well the main anisotropic and magnetoelastic features observed in $Y_2Fe_{14}B$. In fact the sign obtained for the CEF parameter B_{20} agrees with an easy $\boldsymbol{c}$ axis for the system. The irrelevance of the

B_{44} CEF parameter sign for the calculated striction values must be related to the fact that B_{44} does not appear in the energy of the CEF orbital doublet, which are the only model states magnetostrictively active. Finally the absence of S_λ (as defined in equation (10*a*)) in the model differential strains given by equations (13) was fully justified in section 4.

The other most noticeable effect is the observed non-monotonic temperature variations of the strictions $\Delta\epsilon^{\alpha,1}$ and $\Delta\epsilon^{\alpha,2}$, which both peak at about 200 K and then decrease with temperature. This effect seems ubiquitous for Fe rich systems, as also appears in Fe metal [10] and in the intermetallic Y_2Fe_{17} [19]. The explanation of a such decrease naturally comes about from our simple rigid-band Stoner magnetostriction model as follows. For the magnetization set along the hard $\boldsymbol{a}$ axis, when temperature decreases below about 200 K the sub-bands $\lambda = 2$ and 4 (which result from the magnetostrictive $\{|xz\rangle, |yz\rangle\}$ doublet), become, according to our calculations, rapidly populated, which brings about a decrease of the orbital angular momentum $\langle \boldsymbol{L} \rangle$ and thereof of the pure CEF magnetostriction. Meanwhile for the magnetization along the $\boldsymbol{c}$ axis the populations of all doublet bands remain constant, according to our calculations. These population increases are related to the observed corresponding partial depopulation of the singlet band $\lambda = 6$ (coming from the $|xy\rangle$ singlet) and of the non-orbital wide bands.

The third main outcome from the comparison of our model with the experiment is the obtention of *microscopic* MEL coupling parameters, from where to quantify the strength of such a coupling on realistic physical grounds. We should notice that the MEL parameters, although comparable, are of the opposite sign, i.e. $M^\alpha_{i2} = -0.018$ eV/Fe atom and $M^\alpha_{22} =$ +0.0086 eV/Fe. If the assumption $M^\alpha_{i2} = \alpha_L(\partial A_{20}/\partial\epsilon^{\alpha,i})\langle r^2\rangle_{3d}$ $(i = 1, 2)$, as for localized magnetic electrons [12], applies, the equal sign of M^α_{12} and B_{20} is physically correct as the uniform volume strain does not modify the CEF symmetry. However, the ratio c/a is modified under the tetragonal strain and a change of the M^α_{22} parameter sign is possible [12].

We should finally discuss the degree of confidence to be put on the different parameter values ensuing from this work. Our magnetostriction experiment explanation, although reputable, looking at the excellent fittings obtained (figures 3 and 4), is based on a *simplified* model to deal with the formidable task of calculating the rotational α-mode strictions in such a complex system as $Y_2Fe_{14}B$. Therefore the degree of validity should not be extrapolated beyond the boundaries of this simple model, although it is fair to say that most of the ingredients which would require a more sophisticated model are included in ours, in particular within Hamiltonian equation (1). Then within this particular context the parameter values used are correct and accurate enough because they are those giving the 'best' fit to the measured magnetostrictions. We have also seen that the orders of magnitude and signs obtained for the fitted parameters are quite reasonable physically and in good agreement with other available sources. In particular the orders of magnitude and signs of the single-ion microscopic CEF MEL parameters, one of the targets of our work, are rather convincing to us. Nevertheless again we consider our work as a first step on the way to understand the MEL coupling in *itinerant* ferromagnetic metals, as there are certain uniaxial 3d intermetallics, where rotational magnetostriction is larger than in the pure and 'classical' ferromagnets such as iron and nickel [10].

Acknowledgments

We are grateful to Professor D Givord for the provision of the $Y_2Fe_{14}B$ single crystal. Early useful discussions with Dr Clara I Marquina are acknowledged. We acknowledge the Spanish CICYT for the supporting grant No MAT97-1038. CA is grateful to the Diputación General de Aragón (DGA) for the doctorate grant No BCB 94/33. KK and AdM are grateful to the Spanish CICYT for the grant of 'Profesor en Estancia de Año Sabático' No SAB95-0323 (KK).

Appendix A

The magnetoelastic energy contributions to the energy levels of Hamiltonian equation (1) for both orientations of $\boldsymbol{H}_{\rm eff}$, e.g. for the $\epsilon^{\alpha,2}$ mode, are:

$$E^m_{1,2} = E^m_{3,4} = -\left(6M^\alpha_{2,1} - \frac{\sqrt{3}}{2}M^\alpha_{2,2}\right)\epsilon^{\alpha,2} \tag{A1}$$

$$E^m_{5,6} = E^m_{7,8} = -(6M^\alpha_{2,1} - \sqrt{3}M^\alpha_{2,2})\epsilon^{\alpha,2} \tag{A2}$$

$$E^m_{9,10} = -(6M^\alpha_{2,1} - \sqrt{3}M^\alpha_{2,2})\epsilon^{\alpha,2} \tag{A3}$$

where the states $\{|1\rangle, |2\rangle\}$ and $\{|3\rangle, |4\rangle\}$ respectively are related to the unperturbed orbital doublet $\{|xz\rangle, |yz\rangle\}$ and the remainder states, to the three singlets $|xy\rangle$, $|x^2 - y^2\rangle$ and $|2z^2 - x^2 - y^2\rangle$ respectively, in the way mentioned in section 3.1. For the $\epsilon^{\alpha,1}$ mode the above equations stand merely changing $\{M^\alpha_{2,1}, M^\alpha_{2,2}\}$ for $\{M^\alpha_{1,1}, M^\alpha_{1,2}\}$ respectively.

Appendix B

The parameters $A_{ij}(p)$ quoted in equations (12*a*) and (12*b*) are defined as follows

$$A^\alpha_{11} = 6(-C^\alpha_{22}M^\alpha_{11} + C^\alpha_{12}M^\alpha_{21})/\Delta^\alpha$$
$$A^\alpha_{12} = \sqrt{3}(-C^\alpha_{12}M^\alpha_{22} + C^\alpha_{22}M^\alpha_{12})/\Delta^\alpha$$
$$A^\alpha_{21} = 6(C^\alpha_{12}M^\alpha_{11} + C^\alpha_{11}M^\alpha_{21})/\Delta^\alpha$$
$$A^\alpha_{22} = \sqrt{3}(-C^\alpha_{12}M^\alpha_{12} + C^\alpha_{11}M^\alpha_{22})/\Delta^\alpha.$$

References

[1] Brooks H 1940 *Phys. Rev.* **58** 909
Katayama T 1951 *Sci. Rep. Res. Ins. Tohoku Univ.* A **3** 341
Fletcher G C 1954 *Proc. Phys. Soc.* A **67** 505
Fletcher G C 1954 *Proc. Phys. Soc.* A **68** 1066
[2] Kulakowski K and del Moral A 1994 *Phys. Rev.* B **50** 234
[3] Sagawa M, Fujimura S, Togawa N, Yamamoto H and Matsuura Y 1984 *J. Appl. Phys.* **55** 2083
[4] Ibarra M R, Algarabel P A, Alberdi A, Bartolomé J and del Moral A 1987 *J. Appl. Phys.* **61** 3451
Algarabel P A, Ibarra M R, Marquina C I, del Moral A and Zemirli S 1990 *J. Magn. Magn. Mater.* **84** 109
[5] Herbst J F, Croat J J, Pinkerton F E and Yelon W B 1984 *Phys. Rev.* B **29** 4176
[6] Sagawa M, Fujimura S, Yamamoto H, Maatsuura Y and Hiraga K 1984 *IEEE Trans. Magn.* **13** 1584
[7] Givord D, Li H S and de la Bathie R P 1984 *Solid State Commun.* **51** 857
[8] Callen E R and Callen H B 1963 *Phys. Rev.* **129** 578
Callen E R and Callen H B 1963 *Phys. Rev.* **139** A455
[9] Abadía C, del Moral A, Algarabel P A and Kulakowski K 1997 *J. Appl. Phys.* **81** 5702
[10] See Carr W J 1966 *Handbuch der Physik* vol 12, ed S Flügge and H P J Wijn (Berlin: Springer) p 274 and references therein
[11] del Moral A, Algarabel P A and Ibarra M R 1987 *J. Magn. Magn. Mater.* **69** 285 and references therein
[12] del Moral A 1993 *Magnetoelastic Effects and Applications* ed L Lanotte (Amsterdam: Kluwer) p 1
del Moral A, Ibarra M R, Algarabel P A and Arnaudas J I 1991 *Physics of Magnetic Metals* ed W Gorzkowski *et al* (Singapore: World Scientific) p 90
[13] Grössinger R, Sun X K, Eibler R, Buschow K H J and Kirchmayr H R 1985 *J. Physique* **6** C221
Yamada M, Kato H, Yamamoto H and Nakawa Y 1988 *Phys. Rev.* B **38** 620
Radwanski R J and Franse J J M 1989 *J. Magn. Magn. Mater.* **80** 14
[14] See, for instance, a discussion in Gautier F 1982 *Magnetism of Metals and Alloys* ed M Cyrot (Amsterdam: North-Holland) p 1
[15] Sachs M 1963 *Solid State Theory* (New York: McGraw-Hill)

[16] See, e.g., Ashcroft N W and Mermin N D 1976 *Solid State Physics* (Philadelphia, PA: Saunders) p 133
[17] Hutchings M T 1964 *Solid State Physics* **16** 227
Buckmaster H A 1962 *Can. J. Phys.* **40** 1670
[18] Eriksson O, Johansson B, Albers R C, Boring A M and Brooks M S S 1990 *Phys. Rev.* B **42** 2707
[19] Kulakowski K and del Moral A 1995 *Phys. Rev.* B **52** 15 943
[20] Kondorski E I and Straube E 1972 *Zh. Eksp. Teor. Fiz.* **63** 356 (Engl. transl. *Sov. Phys.–JETP* **36** 188)
Mori N 1969 *J. Phys. Soc. Japan* **27** 307
Mori N, Fukuda Y and Ukai T 1974 *J. Phys. Soc. Japan* **27** 1263
[21] Slater J C and Koster G F 1954 *Phys. Rev.* **94** 1498
[22] Gu Zong-Quan and Ching W Y 1987 *Phys. Rev.* B **36** 8530
[23] Shiga M, Kusakabe Y, Nakamura Y, Makita K and Sagawa M 1989 *Physica* B **161** 206
[24] Givord D and Li H S 1985 *Nd–Fe Permanent Magnets: their Present and Future Applications* ed I V Mitchell (London: Elsevier)